Critical role of the motor density and distribution on polar active polymers

Surabhi Jaiswal,* Prithwiraj Maity, and Snigdha Thakur†
Department of Physics, Indian Institute of Science Education and Research Bhopal, Bhopal 462066, India

Marisol Ripoll‡
Theoretical Physics of Living Matter, Institute for Advanced Simulation, Forschungszentrum Jülich, 52425 Jülich, Germany

(Received 15 March 2025; accepted 16 December 2025; published 28 January 2026)

Polar polymer activity underlies numerous cellular processes driven by molecular motors or enzymes. Active polymers with activity on all constituent monomers display compact globular structure, while polymers with only head activity are known to result in stretched configurations. However, most biological and synthetic polymers feature activity localized in just a few sites, a scenario that significantly differs from both previous limits. In this work, we investigate how the density and distribution of motors critically influence the conformational and dynamical properties of polar active polymers. Using overdamped Langevin dynamics simulations, we show that globular conformations for high motor densities change to stretched ones for the more realistic moderate or low density of motors. Interestingly, the polymer's velocity exhibits a nonmonotonic dependence on motor density, with maximum propulsion at intermediate densities. Furthermore, the location of the first motor profoundly impacts polymer conformations; even a slight shift leads to drastic differences between coiled and stretched states. Our findings reveal that motor placement and density govern the structural transitions, characteristic timescales, and propulsion dynamics of polar active polymers, which will have numerous practical implications in the design and understanding of active synthetic and biopolymers.

DOI: 10.1103/j1lq-6phk

I. INTRODUCTION

A large number of crucial biological functions in the cell are governed by polymer activity. Biological polymers become active because of the presence of molecular motors or enzymes, and synthetic polymers might come into contact with active baths or with external activation, such as magnetism or phoretic processes. The genome is organized into highly dynamic chromatin structures that regulate the access to progressive enzymes such as RNA polymerase to transcript encoded genes [1–4]. Cellular filaments such as actin or microtubules move by the action of cytoskeletal molecular motors such as kinesin or myosin [5–7]. In the process, such molecular machinery consumes chemical energy and exerts mechanical forces on the polymer [8–16]. The role of active forces on flexible polymers like chromatin in the context of genome organization, or in semiflexible filaments such as actin and microtubule, is currently being investigated using a variety of theoretical [17,18] and experimental techniques [19–27].

Active polymers have also been investigated from a fundamental perspective by a number of simulation and analytical mesoscopic approaches that incorporate motor activity in different flavors. Driving the polymer out of equilibrium by imposing different temperatures at different monomeric positions [28,29], employing colored noise [30–32], or data-driven procedures where effective equilibrium polymer models optimize the intermonomer interactions to generate structures consistent with the experimental observations [33–36]. Other types of schemes consider the nonequilibrium aspects of how self-propulsion force is locally applied. This can be either without any correlation along the backbone (active Brownian polymers) [37–40] or parallel to the backbone (polar active polymers) [41–51], also in ring polymer configurations [52–56]. In particular, the latter forcing model is similar to the sliding of RNA polymerase on chromatin during transcription [57–59] or molecular motor walking on the microtubule [26,27]. The polar activity on the polymer shows interesting properties that depend on its flexibility as well as its dimensionality [41,60–64].

Most of the theoretical understanding on polar active polymers has until now focused on the case where all constituent monomers are active. With this constraint, it has been shown that the introduction of polar activity systematically reduces the extension of the polymers, resulting even on globulelike structures [41,65,66]. However, for experimental biopolymers, as well as synthetic polymers, activity is typically exerted just on some of the monomers. For example, chromatin transcriptional activity lies within a few segments only along the genome, the genes, and it turns out that approximately 20% of the total genes are transcriptionally active at a given time, leading to only a fraction of the genome experiencing transcriptional activity carried out by RNA

*Contact author: surabhi19@iiserb.ac.in
†Contact author: sthakur@iiserb.ac.in
‡Contact author: m.ripoll@fz-juelich.de

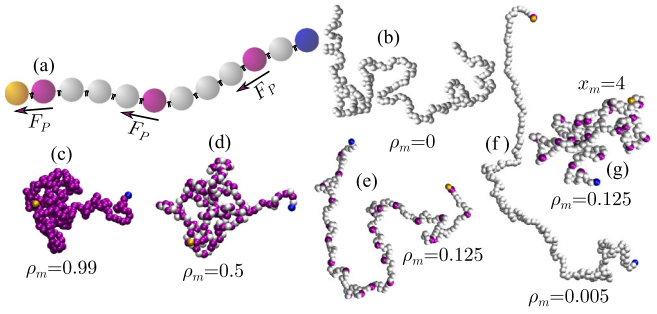

FIG. 1. Polar polymer structure and typical configurations. (a) Polymer sketch with head bead in yellow, motor beads in purple, tail bead in blue, and linker beads in white. The arrows indicate the direction of the polar active force. (b)–(g) Simulation snapshots with $N = 200$. Panel (b) corresponds to the passive case for reference, while snapshots from panels (c) to (f) illustrate globule to stretch conformations with decreasing motor densities ρ_m for the chain length at Pe = 17 and first motor placed in the second bead, $x_m = 2$. See Movie 1 and Movie 2 in the Supplemental Material [67]. (g) Snapshot with the first motor placed in the fourth bead, $x_m = 4$.

polymerase [1]. Cytoskeletal molecular motors like kinesin or myosin attach only to a few spots in each actin or microtubule. Similarly, in the case of synthetic polymers varying the polymer properties by the motor density offers a promising avenue for developing applications. The role played by the density of the motors and their position is therefore of fundamental importance when describing the conformations and dynamics of active polymers. Although how these motors dynamically displace will play a very important role, we focus here first in the case that the motors have fixed positions.

II. MODEL

Linear flexible polymers with polar activity are investigated here with a simulation approach provided by the overdamped Langevin equation. Each polymer is composed of N beads with diameter σ, and consecutive beads connected with harmonic springs and excluded volume interaction among the non-neighboring beads, introduced through the repulsive WCA potential together with an additional soft repulsive force to account for the solvation layer present around each monomer [65] (see the Supplemental Material [67] for details). This solvation layer has shown to be the major effect included by hydrodynamics for polar active polymers when being in the collapse configuration [65,68,69]. In the case of fully stretched polymers, the effect of hydrodynamics is also expected to be negligible [70–72], although for other polymer configurations, the effect of hydrodynamics could be more significant, depending largely on the system. In order to perform a first approach to this system, for this investigation, we consider solely the solvation layer leaving futher investigation of the full solvent effect for future work. The monomers selected as motors have a force $\mathbf{F}_P = -f_c\hat{\mathbf{e}}_j$ pointing toward the previous bead, as depicted in Fig. 1(a). The unit vector $\hat{\mathbf{e}}_j = (\mathbf{r}_j - \mathbf{r}_{j-1})/|\mathbf{r}_j - \mathbf{r}_{j-1}|$ with $\mathbf{r}_j$ the position of motor j. Therefore, the very first bead cannot have a motor and the number of motors N_m can vary between 0 and $N - 1$, such that the density of the motors is $\rho_m = N_m/N$, with $\rho_m = 0$ corresponding to the passive polymer [see Fig. 1(b)] and $\rho_m = 0.99$ to the case where all beads but the first are active [see Fig. 1(c)]. We show that how the introduction of the motor density is necessary to explain the dynamics of active polymers as a crossover between these two limits, similar to the concept of semiflexibility was necessary to characterize the behavior of passive polymers between the rigid and the fully flexible limits.

First, the motors are uniformly distributed along the polymer, and the position of first motor is placed in the second bead, which we denote as $x_m = 2$, completely at the head; see Figs. 1(c)–1(f) for representative values of ρ_m. Later, we also consider the nonuniform distribution case, and different positions for the first motor; see one case in Fig. 1(g). A random initial configuration is considered and the simulation is run until steady state is reached. Activity can be characterized in terms of the monomeric Péclet number, $\mathrm{Pe} = f_c b/k_\mathrm{B}T$, with k_B is the Boltzmann constant and T is the temperature of the system. This definition of Pe refers to the ratio of locally applied active force and thermal fluctuations and has shown to be the right quantity to describe the polymer deformation induced by polar activity [45].

III. RESULTS

A. Conformational properties

In the limit of full activity, the polymers have been characterized to coil into structures more compact than equilibrium, while in the single head motor limit the structures get stretched [41,45,73–75], as shown also in Fig. 1. The intermediate densities get compactified or stretched depending not only on ρ_m but also on Pe, which occurs independently on the polymer length. In order to quantify the conformational changes, we calculate the radius of gyration $R_g^2 \equiv \sum_{i=1}^{N} (\mathbf{r}_i - \mathbf{r}_\mathrm{cm})^2/N$, where $\mathbf{r}_\mathrm{cm}$ is the center-of-mass position of the polymer and $\mathbf{r}_i$ the position of ith bead. Figure 2(a) shows the averaged R_g in steady state as a function of the motor density in the main plot and as a function of the activity in the inset. The data are normalized with the value at equilibrium, R_{g0}, which makes a clear distinction between compactified and stretched configurations. At lower activity values ($\mathrm{Pe} \lesssim 7$), polymers tend to adopt slightly more compact structures even at low motor densities. In contrast, at higher activities ($\mathrm{Pe} \gtrsim 17$), the chains remain stretched up to relatively large numbers of motors per chain, with the degree of stretching increasing further with activity. It is only all-beads-motor case that compactification increases with activity. A linear interpolation between the fully extended case, $\rho_m \to 0$ (single motor), and the compact case, $\rho_m \to 1$ (all-beads motor) is drawn for reference in Fig. 2(a). This interpolation shows to reasonably explain the dependence of R_g with ρ_m in the limit of infinite activity.

The dependence of the radius of gyration with the polymer size is shown in Fig. 2(b), where a clear power law dependence $\langle R_g \rangle \sim N^\nu$ can be identified for each value of the motor density and the Péclet, with values summarized in Fig. 2(c). Note that a different choice of the Pe would not have resulted in this scaling, which indicates that the monomeric Péclet number is the right quantity [45]. Also, the one motor case does not correspond to a well-defined density, such that

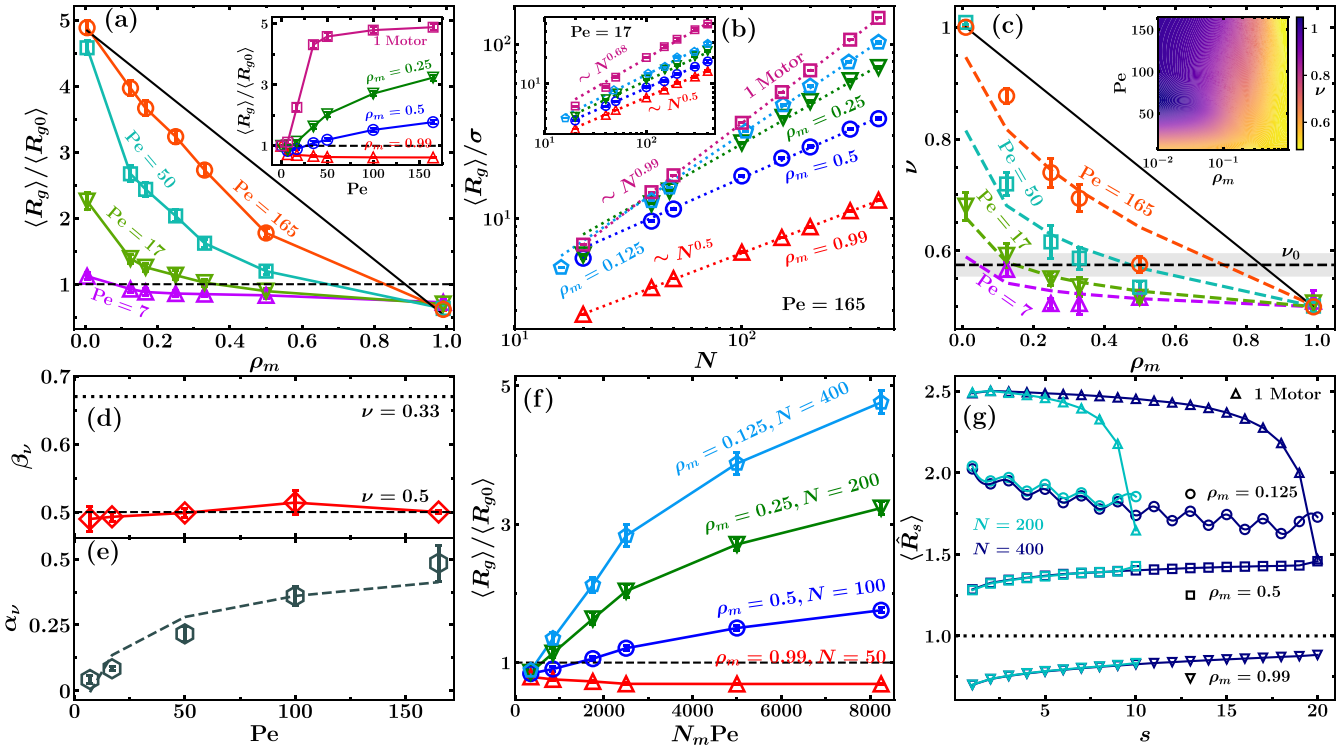

FIG. 2. Conformational stretching and collapsing polymer properties. (a) Averaged radius of gyration normalized by the equilibrium value for $N = 200$ as a function of the motor density in the main plot and of the Péclet number in the inset. (b) Polymer size dependence of $\langle R_g \rangle$ for Pe = 165 in the main plot and Pe = 17 in the inset. Dotted lines are a fit to $\langle R_g \rangle \sim N^\nu$ to determine ν. (c) Flory exponent ν as a function of motor density ρ_m for various Pe values. Lines are the fits with Eq. (1). The inset shows a state diagram with the same data represented in ρ_m, Pe plane. (d), (e) Correspond to the prefactor β_ν and exponent α_ν values as fitted in panel (c). In panel (d), the dashed line is a fit to $\beta_\nu \simeq 0.5$ and in panel (e) to Eq. (2), the dotted line in panel (d) is a guide to the eye to the compact collapse behavior. (f) $\langle R_g \rangle$ as a function of the total applied force N_mPe in four comparable cases with fixed $N_m = 50$ and varying Pe. (g) Mean normalized segment size along the chain contour, with s the segment number and $s = 1$ corresponding to the head for Pe = 50, for various motor densities and two values of the polymer length. In panels (a), (c), and (f) lines connecting points are a guide to the eye and the dashed line is the reference to the equilibrium value. In (a) and (c) the solid black lines connect the fully extended and the collapsed limits for $\rho_m \to 0$ (one motor case) and $\rho_m \to 1$ (all beads motor case), respectively. See Movie 1 and Movie 2 in Supplemental Material [67].

we have approximated this limiting case with $\rho_m \simeq 0.01$. In equilibrium, the exponent ν is known as the Flory exponent and a theoretical prediction simply considering a balance of entropic elasticity and excluded volume interactions that for a three-dimensional polymer results in $\nu_0 = 0.588$ [76]. We measure here $\nu_0 = 0.575 \pm 0.02$, which agrees within the error with the theoretical prediction. A perfectly compact polymer has $\nu_c = 0.33$ by construction, and a perfectly stiff polymer $\nu_s = 1$. This seems to indicate that cases with $\nu < \nu_0$ should correspond to compact states, while cases with $\nu > \nu_0$ should relate to stretched states. Previous studies of polar polymers in the all motor case have verified this extent with compact structures with $\nu < \nu_0$ [41,66]. Our results in Fig. 2(c) show that this is a good estimation, but interestingly, it is not always exactly fulfilled. There are a few cases, such as $\rho_m = 0.25$, Pe = 17, for which $\nu < \nu_0$ although the polymers are getting a slightly stretched with respect to equilibrium.

The dependence of the Flory exponent with activity and motor density can be described by

$$\nu(\mathrm{Pe}, \rho_m) = 1 - \beta_\nu \rho_m^{\alpha_\nu}, \tag{1}$$

where β_ν and α_ν are in principle both functions of Pe. The obtained fitted curves in Fig. 2(c) show a good agreement with the simulation results. The function $\beta_\nu(\mathrm{Pe})$ determines the all-bead motor case ($\rho_m \to 1$). The perfectly compact limit corresponds to $\beta_c = 0.67$, the simulations in Fig. 2(d) show to saturate in a constant $\beta_\nu \simeq 0.5$, which allows fluctuations in the chain configuration. Meanwhile, previous results, without the here employed solvation soft repulsion layer, have shown some Pe dependence [37,41,77]. And note that the limit $\rho_m \to 0$ properly corresponds to the expected behavior for the still active one motor case. The exponential function $\alpha_\nu(\mathrm{Pe})$ in Eq. (1) can be described by

$$\alpha_\nu(\mathrm{Pe}) = 1 - \beta_\alpha \mathrm{Pe}^{\alpha_\alpha}, \tag{2}$$

where the fit in Fig. 2(e) allows us to determine $\beta_\alpha \simeq 1.4$ and $\alpha_\alpha \simeq -0.17$. In this way, the limit of Pe $\to \infty$ can be understood as a linear interpolation between the ν of the limiting fully extended chain and the compact one, which is shown in Fig. 2(c) for reference.

Besides the monomeric Péclet number, the activity can be evaluated by the total force applied on a polymer, this is N_mPe, which can also be related to the total energy consumption.

For a given size of the polymer, this total force can be varied either by changing ρ_m or by changing Pe. In principle, an overall effective stretching could have been directly related to this total force, but Fig. 2(f) shows otherwise, and makes obvious that with the same energy consumption and the same number of motors the stretching is larger the larger the chain, which might not be intuitive at first. Similarly, the inset of Fig. 2(a) already shows that given the same activity and the same polymer length, the stretching is larger the smaller the number of motors.

Local conformations have also shown to be importantly affected by polar activity in the single polymer case [45], as well as in melt conditions [46]. Figure 2(g) depicts $\langle \hat{R}_s \rangle$, the end-to-end distance of polymer segments with $N_s = 20$ monomers along the contour length, normalized with the segment size in equilibrium. For the all-motor case, $\rho_m = 0.99$, the head is clearly more compact than the tail, which corresponds to the already reported polar activity induced polymer progressive deformation [45,46]. The tension induced by each motor accumulates along the chain, due to the polarity of the force, such that at the head with almost no tension, the rotational diffusion makes the chain more flexible; while at the tail the large accumulated tension makes the chain stiffer. This trend is maintained for the case where every second bead is active, $\rho_m = 0.5$, although in this case, the segments have stretched with respect to equilibrium, $\langle \hat{R}_s \rangle > 1$, in contrast to the all active case where they were the segments have got more compact, $\langle \hat{R}_s \rangle < 1$. A further decrease in motor density reverses this trend and the stretching monotonously decreases toward the tail, an effect that becomes more prominent the smaller the number of motors (the oscillations for $\rho_m = 0.125$ are due to the different number of motors in consecutive segments). Increasing the separation between motors decreases the tension along the chain due to the intrinsic chain fluctuations, which is particularly clear for the single-motor case where the tail is completely dangling, and explains the change of trend. Furthermore, the overall behavior of $\langle \hat{R}_s \rangle$ is independent of N, besides some deviation for the last segment due to the difference in tension. The main conclusions drawn here are qualitatively the same with different values of the applied activities, as can be seen in Fig. S1 in the Supplemental Material [67]. Therefore, polar activity breaks down the polymer self-similar scaling behavior in a very consistent manner, with a change of trend from head coiled to head extended that occurs around $\rho_m \simeq 0.25$, this is for polymers with one motor every fourth bead, which, to our understanding, is still a large density of motors. We further characterized the polymer conformations by quantifying the spatial correlation function of the bond vector $\beta(l) = \langle \mathbf{n}_i \cdot \mathbf{n}_{i+l} \rangle$, where $\mathbf{n}_i = (\mathbf{r}_{i+1} - \mathbf{r}_i)/|\mathbf{r}_{i+1} - \mathbf{r}_i|$ is the normalized tangent vector at the position of the beads $\mathbf{r}_i$, along the polymer contour $l \in (1, \ldots, N-1)$. The brackets indicate the average over the initial bead i, and configurations in the steady state corresponding to different times and realizations. When the bonds are parallel on average, $\beta(l) = 1$, and when antiparallel $\beta(l) = -1$ [78]. The bond correlation is depicted in Fig. 3 for different values of ρ_m and Pe. The dotted line for $\rho_m = 0$ represents an exponential decay of the correlation for the reference equilibrium case. The decay of the correlation is progressively slower with increasing values of Pe, as shown in the inset of Fig. 3, highlighting the increase of stretching with activity at this moderate density of motors, which can be interpreted as an activity-induced stiffness. Similar behavior is observed with lower motor densities with a stretching response to activity if found, but not for higher motor densities where activity results in compactification. Figure 3 shows how decreasing the density of motor slows down the decay of the correlation. Negative values of $\beta(l)$, with a characteristic length at the minimum value of correlation, are observed for $\rho_m = 0.99$ and for $\rho_m = 0.5$, indicating the formation of multiple hairpins that lead to collapsed structures. For $\rho_m = 0.125$, oscillations similar to a curtain-hanging band are observed in Fig. 3, with an overall clear decay along longer segments of the polymer contour. These oscillations are related to the presence of the motors; the segments in between motors show a fast decorrelation, which increases for the next motor. Consecutive motors keep a higher correlation, which finally also decays along the polymer contour, as can also be seen in the snapshot in Fig. 1(e).

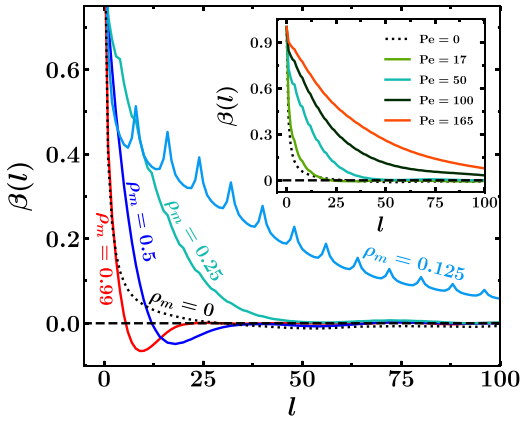

FIG. 3. Bond vector correlation $\beta(l)$ decay along l, the polymer contour, for $N = 400$. The main plot shows various values of the density of the motor ρ_m for active polymers with Péclet number, Pe = 50. The inset shows various values of Pe at $\rho_m = 0.25$.

B. Dynamic properties

The dynamic behavior of the polar active polymer is also importantly affected by the motor density. We quantify this effect in two ways. First, the time evolution from an arbitrary initial state to the final steady state under polar activity allows us to determine the characteristic steady-configurational time τ_s with

$$\frac{\langle R_g(t) \rangle}{\langle R_g \rangle} = 1 - a_1 \exp[-(t/\tau_s)], \tag{3}$$

where $a_1 = 1 - R_g(0)/\langle R_g \rangle$ is a constant determined by the initial configuration $R_g(0)$, such that τ_s is now the only fitting parameter [79]. The time evolution of the normalized radius of gyration is displayed in the inset of Fig. 4(a) for different motor densities at Pe = 165 for $N = 100$. Higher density of motors imparts the higher activity to the polymer making the evolution faster and therefore reducing τ_s. Figure 4(a) shows that τ_s decreases with increasing Pe and ρ_m, this is with increasing local activity and motor density.

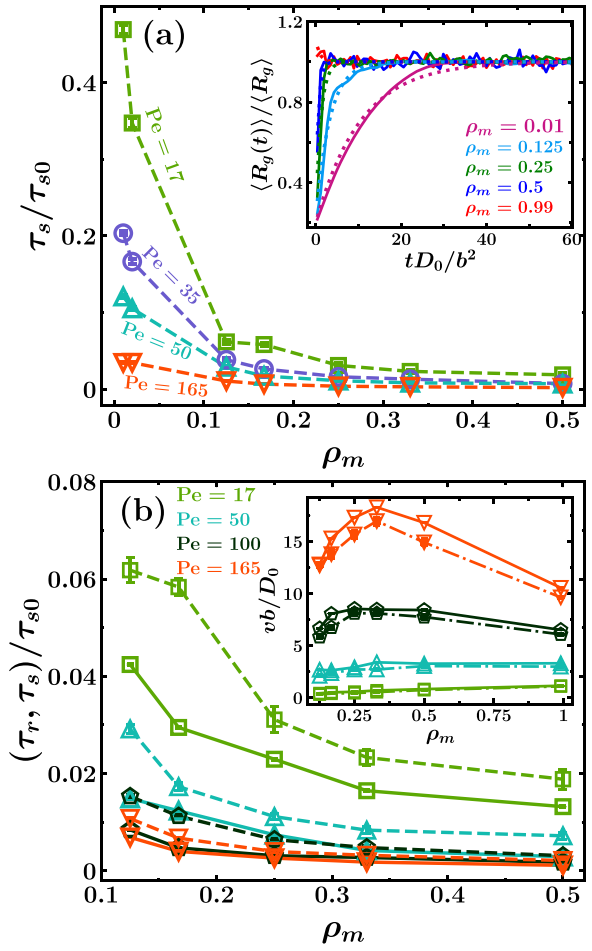

FIG. 4. Dynamic polar polymer properties. (a) Characteristic steady-configurational time τ_s as a function of motor density, for $N = 100$, normalized by the equilibrium value τ_{s0}. The inset displays time-dependent average radius of gyration for various motor densities, where the dotted lines correspond to Eq. (3), with τ_s as a fitting parameter, for $N = 100$ and $\mathrm{Pe} = 165$. (b) Characteristic rotational time τ_r as obtained from the mean square displacement (MSD) for $N = 400$ (solid lines), compared with a zoom of the data in panel (a) for τ_s (dashed lines). The inset corresponds to the polymer center-of-mass velocity as obtained from the MSD for $N = 400$ (solid lines). Dashed-dotted lines in the inset correspond to the velocity estimation in terms of the effective force as, $vb/D_0 = \rho_m \mathrm{Pe} R_e/(Nb)$, where R_e is the end-to-end polymer distance. Time and velocity are given in units of the monomer bond length b, and the equilibrium single monomer diffusion coefficient D_0 (see details in Supplemental Material [67]). See Movie 1 and Movie 2 in the Supplemental Material [67].

The second characterization of the polymer dynamics is performed through the center-of-mass MSD calculated in the steady state for different densities and Pe values. The MSD shows the typical behavior of an active Brownian particle [45,80,81] with a long-time ballistic regime followed by a diffusive regime (see Fig. S2 in the Supplemental Material [67]). This enables the determination of the polymer self-propulsion velocity v and the characteristic rotational time τ_r, both displayed in Fig. 4(b). The characteristic rotational time decreases with increasing Pe, which relates to the faster reorientation of the trajectories with increasing activity. Increasing the density of motors also decreases the local and global reorientation of the polymer, which results in smaller values of τ_r. For comparison, Fig. 4(b) also includes a zoomin of the values for τ_s, which show to be very similar. The differences can be related to the variation of polymer length between the two data sets. The fact that the two characteristic times τ_s and τ_r are essentially the same indicates that in the presence of polar activity, there is a unique typical characteristic time which decreases with activity and motor density.

The self-propulsion velocity v, in the inset of Fig. 4(b), increases monotonically with Pe for all densities, as expected. On the other hand, the dependence on motor density for a given Pe is nonmonotonic. To understand this effect, the effective force acting on the polymer center of mass, F_e, needs to be considered. The total applied force, $N_m \mathrm{Pe}$, increases both with ρ_m and Pe, but this force directly determines the polymer velocity only in the case of total stretching. For all polymer structures, the velocity is determined by F_e and the total polymer friction; this is $v = F_e/(N\mu)$, with $\mu = k_B T/D_0$ the friction on a single monomer, and $F_e = \rho_m R_e \mathrm{Pe}$, with R_e the measured polymer end-to-end distance. The inset of Fig. 4(b) shows that this approximation explains the velocity dependence very well. For large values of the activity, maximum propulsion is therefore achieved at a particular intermediate motor density. Decreasing the value of the activity, the nonmonotonicity also decreases, and for relatively small Pe values, the velocity increases slowly and monotonically with increasing motor density. While the motor density has been shown to critically influence the properties of polar polymers, how these motors are distributed along the chain is also crucial. For a fixed motor density, $\rho_m = 0.125$ at high activity value $\mathrm{Pe} = 165$, we compare the homogeneous distribution of motors considered until now, with a random distribution of motors, and sort the results according to the position of the first motor, x_m. For reference, we also perform simulations for the homogeneous case with varying location of the first motor. The inset of Fig. 5 shows how the average radius of gyration drastically depends on x_m. When the first motor is at the head, $x_m = 2$, the polymer is basically completely stretched, while placing the first motor just one position behind; i.e., $x_m = 3$ shows a drastic difference that indicates the polymer is not anymore stretched but in a clearly much more coiled configuration. Increasing the number of passive monomers in front of the first motor, i.e., enlarging x_m, intensifies the trend of the polymer to coil into more compact structures. Passive monomers in front of the first motor help the head to lose its directionality, which frequently randomizes the motion of the subsequent motors, eventually leading to coiled states.

C. Non-homogeneous motors distribution

For the case with random distribution of motors, the differences among different configurations are large such that we evaluate the actual sizes by the radius of the gyration probability distribution function, as shown in the main panel of Fig. 5. The plethora of possible random conformations clearly widens the R_g distribution for the random configurations as compared to the uniform ones, which is especially drastic for $x_m = 2$, when the first motor is placed at the head position. Snapshots of example configurations are depicted in Fig. 5,

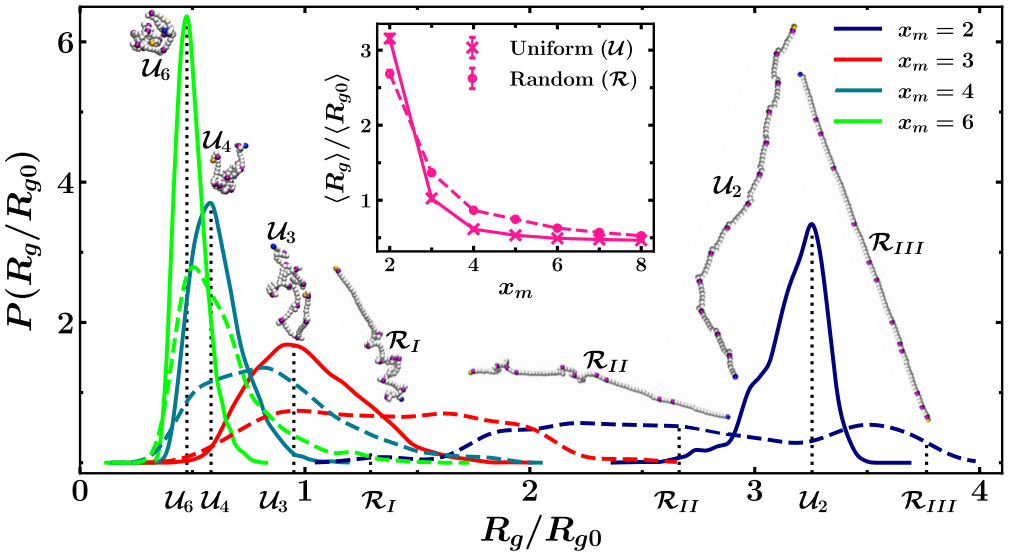

FIG. 5. Probability distribution of the normalized radius of gyration for active polymers with uniformly (solid lines) and randomly (dashed lines) distributed motors with $\rho_m = 0.125$, $N = 100$, and Pe $= 165$. The position of the first motor is fixed at different positions x_m (see Movie 3 in the Supplemental Material [67]). The inset plot shows the variation of $\langle R_g\rangle/\langle R_{g0}\rangle$ with x_m. The snapshots represent polymer typical conformations, with radius of gyration indicated by the dotted lines. $\mathcal{U}$ and $\mathcal{R}$ denote, respectively, uniform and random configurations. Various values of the first motor position, x_m, are displayed for $\mathcal{U}_m$ configurations, while all $\mathcal{R}$ have $x_m = 2$ (see Movie 4 and Movie 5 in the Supplemental Material [67]).

where $\mathcal{U}_m$ denotes configurations with a uniform distribution of motors at a given value of x_m. The difference between $\mathcal{U}_2$ (with $x_m = 2$) and $\mathcal{U}_3$ (with $x_m = 3$) illustrates the much more coiled structures when one-single dangling monomer is placed in front of the first motor. The snapshots denoted as $\mathcal{R}$ are representative random configurations, all with $x_m = 2$. $\mathcal{R}_{\rm III}$ shows how an accumulation of motors close to the head leads to an overall stretched configuration, while $\mathcal{R}_{\rm II}$ and $\mathcal{R}_{\rm I}$ show that the accumulation at different places in the chain leads to coiled segments, resulting in more or less compact configurations. These effects persist for $x_m > 2$, as indicated by the width of radius of gyration probability distributions, although the differences between random and homogeneous become less pronounced with increasing x_m, such that for $x_m = 6$ only a reminiscent difference persists. Finally, note that although we have here focused on a particular set of parameters, we expect that qualitatively similar conclusions can be drawn for a wide range of values. Smaller values of Pe are, for example, expected to show differences in stretching, although less obvious than the ones discussed here. Smaller values of ρ_m are expected to show wider distributions of the radius of gyration, similar to larger values of N, which might also display a slightly different behavior with x_m.

IV. DISCUSSION

In conclusion, the density and location of the active sites play a major role in determining the conformational and dynamical behavior of polar active polymers. Compact coiled structures are to be found for polymers with a very large density of motors, and interestingly also for lower densities of motors, but only for cases in which a number of passive dangling monomers are placed before the first motor. The change from compact to stretched configurations typically occurs at $\rho_m \simeq 0.25$, this is for polymers with one motor every fourth bead, which can be considered a relatively high motor density. Self-similarity is typically lost in the presence of polar activity, and this can change from coiled head and stiff tail for the cases with very large density of motor, to the opposite stiff head and coiled tail for the cases with lower density of motors. While the rotational characteristic times decrease with increasing local activity and number of motors, the self-propelled velocities also account for the total polymer extension, such that nonmonotonic dependencies are found for large values of the local activity. The change from homogeneous to random motor distribution has extreme consequences in the polymers configuration and dynamics, being the position of the first motor in the chain the most determinant factor. A shift of the first motor from the head by a few beads back can drastically change the chain typical configurations from fully extended to largely coiled. An activity-induced stiffening is therefore characteristic of fully flexible linear polymers with polar activity on only a fraction of the monomers, and propulsion initiated at the polymer head, which will be larger not only for increasing local activity, but also for decreasing motor density. Other effects not considered here, such as chain rigidity, motor displacement along the chain, or hydrodynamic interactions are expected to modify some of the results here discussed, although it is to be expected that the first approach here considered sets a general validity and solid reference frame. Our observations have numerous practical implications relevant in diverse fields, such as the design of synthetic phoretic active polymers, or the understanding of mechanisms related to molecular motors like RNA polymerase on biopolymers. In particular, our results can, for example, explain the reason why biologically relevant polymers like chromatin

might change from a larger number of motors with lower activity to a lower number of motors with high activity when the transcriptional activity needs to be increased.

ACKNOWLEDGMENTS

S.J. thanks a research fellowship from UGC India. S.T. acknowledges SERB India for research Grant No. CRG/2022/003778. The authors would like to acknowledge the HPC facility at IISER Bhopal for allocating the necessary computational resources. The authors gratefully acknowledge the computing time granted by the JARA Vergabegremium and provided on the JARA Partition part of the supercomputer JURECA at Forschungszentrum Jülich [82].

DATA AVAILABILITY

The data are available from the authors upon reasonable request.

[1] B. Lewin, *Genes IX* (Jones & Bartlett Learning, Burlington, MA, 2008), Vol. 9.

[2] L. Zhang, D.-A. Silva, F. Pardo-Avila, D. Wang, and X. Huang, Structural model of RNA polymerase II elongation complex with complete transcription bubble reveals NTP entry routes, PLoS Comput. Biol. **11**, e1004354 (2015).

[3] E. P. Geiduschek and G. P. Tocchini-Valentini, Transcription by RNA polymerase III, Annu. Rev. Biochem. **57**, 873 (1988).

[4] L. Bai, T. J. Santangelo, and M. D. Wang, Single-molecule analysis of RNA polymerase transcription, Annu. Rev. Biophys. Biomol. Struct. **35**, 343 (2006).

[5] D. Mizuno, C. Tardin, C. F. Schmidt, and F. C. MacKintosh, Nonequilibrium mechanics of active cytoskeletal networks, Science **315**, 370 (2007).

[6] D. Humphrey, C. Duggan, D. Saha, D. Smith, and J. Käs, Active fluidization of polymer networks through molecular motors, Nature (London) **416**, 413 (2002).

[7] A. Yildiz, M. Tomishige, R. D. Vale, and P. R. Selvin, Kinesin walks hand-over-hand, Science **303**, 676 (2004).

[8] C. Y. Zhou, S. L. Johnson, N. I. Gamarra, and G. J. Narlikar, Mechanisms of ATP-dependent chromatin remodeling motors, Annu. Rev. Biophys. **45**, 153 (2016).

[9] Z. Cao and P. G. Wolynes, Motorized chain models of the ideal chromosome, Proc. Natl. Acad. Sci. USA **121**, e2407077121 (2024).

[10] D. Needleman and Z. Dogic, Active matter at the interface between materials science and cell biology, Nat. Rev. Mater. **2**, 17048 (2017).

[11] B. van Steensel and E. E. Furlong, The role of transcription in shaping the spatial organization of the genome, Nat. Rev. Mol. Cell Biol. **20**, 327 (2019).

[12] K. Struhl and E. Segal, Determinants of nucleosome positioning, Nat. Struct Mol. Biol. **20**, 267 (2013).

[13] G. Fudenberg, M. Imakaev, C. Lu, A. Goloborodko, N. Abdennur, and L. A. Mirny, Formation of chromosomal domains by loop extrusion, Cell Rep. **15**, 2038 (2016).

[14] M. Dogterom and G. H. Koenderink, Actin–microtubule crosstalk in cell biology, Nat. Rev. Mol. Cell Biol. **20**, 38 (2019).

[15] M. P. López, F. Huber, I. Grigoriev, M. O. Steinmetz, A. Akhmanova, G. H. Koenderink, and M. Dogterom, Actin–microtubule coordination at growing microtubule ends, Nat. Commun. **5**, 4778 (2014).

[16] L. Bourdieu, T. Duke, M. B. Elowitz, D. A. Winkelmann, S. Leibler, and A. Libchaber, Spiral defects in motility assays: A measure of motor protein force, Phys. Rev. Lett. **75**, 176 (1995).

[17] N. Gupta, A. Chaudhuri, and D. Chaudhuri, Morphological and dynamical properties of semiflexible filaments driven by molecular motors, Phys. Rev. E **99**, 042405 (2019).

[18] A. Shee, N. Gupta, A. Chaudhuri, and D. Chaudhuri, A semiflexible polymer in a gliding assay: Reentrant transition, role of turnover and activity, Soft. Matter **17**, 2120 (2021).

[19] A. Goychuk, D. Kannan, A. K. Chakraborty, and M. Kardar, Polymer folding through active processes recreates features of genome organization, Proc. Natl. Acad. Sci. USA **120**, e2221726120 (2023).

[20] A. L. Sanborn, S. S. P. Rao, S.-C. Huang, N. C. Durand, M. H. Huntley, A. I. Jewett, I. D. Bochkov, D. Chinnappan, A. Cutkosky, J. Li, K. P. Geeting, A. Gnirke, A. Melnikov, D. McKenna, E. K. Stamenova, E. S. Lander, and E. L. Aiden, Chromatin extrusion explains key features of loop and domain formation in wild-type and engineered genomes, Proc. Natl. Acad. Sci. USA **112**, E6456 (2015).

[21] E. Lieberman-Aiden, N. L. Van Berkum, L. Williams, M. Imakaev, T. Ragoczy, A. Telling, I. Amit, B. R. Lajoie, P. J. Sabo, M. O. Dorschner, *et al.*, Comprehensive mapping of long-range interactions reveals folding principles of the human genome, Science **326**, 289 (2009).

[22] D. W. Heermann, Physical nuclear organization: Loops and entropy, Curr. Opin. Cell Biol. **23**, 332 (2011).

[23] J. Mateos-Langerak, M. Bohn, W. de Leeuw, O. Giromus, E. M. M. Manders, P. J. Verschure, M. H. G. Indemans, H. J. Gierman, D. W. Heermann, R. van Driel, and S. Goetze, Spatially confined folding of chromatin in the interphase nucleus, Proc. Natl. Acad. Sci. USA **106**, 3812 (2009).

[24] R. K. Sachs, G. van den Engh, B. Trask, H. Yokota, and J. E. Hearst, A random-walk/giant-loop model for interphase chromosomes, Proc. Natl. Acad. Sci. USA **92**, 2710 (1995).

[25] S. S. Rao, M. H. Huntley, N. C. Durand, E. K. Stamenova, I. D. Bochkov, J. T. Robinson, A. L. Sanborn, I. Machol, A. D. Omer, E. S. Lander, and E. L. Aiden, A 3D map of the human genome at Kilobase resolution reveals principles of chromatin looping, Cell **159**, 1665 (2014).

[26] Q. Wen and P. A. Janmey, Polymer physics of the cytoskeleton, Curr. Opin. Solid State Mater. Sci. **15**, 177 (2011).

[27] R. M. Robertson-Anderson, *Biopolymer Networks* (IOP Publishing, Bristol, UK, 2024).

[28] A. Agrawal, N. Ganai, S. Sengupta, and G. I. Menon, Nonequilibrium biophysical processes influence the large-scale architecture of the cell nucleus, Biophys. J. **118**, 2229 (2020).

[29] J. Smrek, I. Chubak, C. N. Likos, and K. Kremer, Active topological glass, Nat. Commun. **11**, 26 (2020).

[30] A. Ghosh and N. Gov, Dynamics of active semiflexible polymers, Biophys. J. **107**, 1065 (2014).
[31] D. Osmanović and Y. Rabin, Dynamics of active rouse chains, Soft Matter **13**, 963 (2017).
[32] S. Brahmachari, T. Markovich, F. C. MacKintosh, and J. N. Onuchic, Temporally correlated active forces drive segregation and enhanced dynamics in chromosome polymers, PRX Life **2**, 033003 (2024).
[33] Q. MacPherson, B. Beltran, and A. J. Spakowitz, Bottom–up modeling of chromatin segregation due to epigenetic modifications, Proc. Natl. Acad. Sci. USA **115**, 12739 (2018).
[34] M. Chiang, D. Michieletto, C. A. Brackley, N. Rattanavirotkul, H. Mohammed, D. Marenduzzo, and T. Chandra, Polymer modeling predicts chromosome reorganization in senescence, Cell Rep. **28**, 3212 (2019).
[35] G. Shi and D. Thirumalai, From Hi-C contact map to three-dimensional organization of interphase human chromosomes, Phys. Rev. X **11**, 011051 (2021).
[36] S. Fujishiro and M. Sasai, Generation of dynamic three-dimensional genome structure through phase separation of chromatin, Proc. Natl. Acad. Sci. USA **119**, e2109838119 (2022).
[37] A. Kaiser, S. Babel, B. ten Hagen, C. von Ferber, and H. Löwen, How does a flexible chain of active particles swell? J. Chem. Phys. **142**, 124905 (2015).
[38] A. Martín-Gómez, T. Eisenstecken, G. Gompper, and R. G. Winkler, Active Brownian filaments with hydrodynamic interactions: Conformations and dynamics, Soft Matter **15**, 3957 (2019).
[39] S. K. Anand and S. P. Singh, Conformation and dynamics of a self-avoiding active flexible polymer, Phys. Rev. E **101**, 030501 (2020).
[40] S. M. Mousavi, G. Gompper, and R. G. Winkler, Active bath-induced localization and collapse of passive semiflexible polymers, J. Chem. Phys. **155**, 044902 (2021).
[41] V. Bianco, E. Locatelli, and P. Malgaretti, Globulelike conformation and enhanced diffusion of active polymers, Phys. Rev. Lett. **121**, 217802 (2018).
[42] S. K. Anand and S. P. Singh, Structure and dynamics of a self-propelled semiflexible filament, Phys. Rev. E **98**, 042501 (2018).
[43] C. A. Philipps, G. Gompper, and R. G. Winkler, Tangentially driven active polar linear polymers—an analytical study, J. Chem. Phys. **157**, 194904 (2022).
[44] S. Kumar, R. Padinhateeri, and S. Thakur, Shear flow as a tool to distinguish microscopic activities of molecular machines in a chromatin loop, Soft Matter **20**, 6500 (2024).
[45] A. R. Tejedor, J. Ramírez, and M. Ripoll, Progressive polymer deformation induced by polar activity and the influence of inertia, Phys. Rev. Res. **6**, L032002 (2024).
[46] J. Oller-Iscar, A. R. Tejedor, M. Ripoll, and J. Ramírez, Computational study of active polar polymer melts: From active reptation to activity induced local alignment, Polymer **320**, 128074 (2025).
[47] L. van Steijn, M. Fazelzadeh, and S. Jabbari-Farouji, Conformation and dynamics of wet externally actuated filaments with tangential active forces, Phys. Rev. E **110**, 064504 (2024).
[48] R. Sinaasappel, M. Fazelzadeh, T. Hooijschuur, Q. Di, S. Jabbari-Farouji, and A. Deblais, Locomotion of active polymerlike worms in porous media, Phys. Rev. Lett. **134**, 128303 (2025).
[49] A. Panda, R. G. Winkler, and S. P. Singh, Activity-enhanced shear thinning of flexible linear polar polymers, Phys. Rev. E **111**, 055413 (2025).
[50] R. G. Winkler, Conformational properties of active polar semiflexible phantom polymers, J. Chem. Phys. **162**, 154903 (2025).
[51] D. Breoni, C. Kurzthaler, B. Liebchen, H. Löwen, and S. Mandal, Giant activity-induced elasticity in entangled polymer solutions, Nat. Commun. **16**, 5305 (2025).
[52] S. M. Mousavi, G. Gompper, and R. G. Winkler, Active Brownian ring polymers, J. Chem. Phys. **150**, 064913 (2019).
[53] E. Locatelli, V. Bianco, and P. Malgaretti, Activity-induced collapse and arrest of active polymer rings, Phys. Rev. Lett. **126**, 097801 (2021).
[54] S. Kumar and S. Thakur, Local polar and long-range isotropic activity assisted swelling and collapse dynamics of an active ring polymer, Macromolecules **56**, 5229 (2023).
[55] R. G. Winkler and S. P. Singh, Active polar ring polymer in shear flow—An analytical study, J. Chem. Phys. **161**, 064902 (2024).
[56] A. Lamura, Excluded volume effects on tangentially driven active ring polymers, Phys. Rev. E **109**, 054611 (2024).
[57] D. Tenenbaum, K. Inlow, L. J. Friedman, A. Cai, J. Gelles, and J. Kondev, RNA Polymerase sliding on DNA can couple the transcription of nearby bacterial operons, Proc. Natl. Acad. Sci. USA **120**, e2301402120 (2023).
[58] B. Alberts, A. Johnson, J. Lewis, M. Raff, K. Roberts, and P. Walter, *Molecular Biology of the Cell* (Garland Science, New York, NY, 2002).
[59] R. K. Zia, J. Dong, and B. Schmittmann, Modeling translation in protein synthesis with TASEP: A tutorial and recent developments, J. Stat. Phys. **144**, 405 (2011).
[60] V. Schaller, C. Weber, C. Semmrich, E. Frey, and A. R. Bausch, Polar patterns of driven filaments, Nature (London) **467**, 73 (2010).
[61] A. Sciortino, L. J. Neumann, T. Krüger, I. Maryshev, T. F. Teshima, B. Wolfrum, E. Frey, and A. R. Bausch, Polarity and chirality control of an active fluid by passive nematic defects, Nat. Mater. **22**, 260 (2023).
[62] K. R. Prathyusha, S. Henkes, and R. Sknepnek, Dynamically generated patterns in dense suspensions of active filaments, Phys. Rev. E **97**, 022606 (2018).
[63] M. Vatin, S. Kundu, and E. Locatelli, Conformation and dynamics of partially active linear polymers, Soft Matter **20**, 1892 (2024).
[64] R. E. Isele-Holder, J. Elgeti, and G. Gompper, Self-propelled worm-like filaments: Spontaneous spiral formation, structure, and dynamics, Soft Matter **11**, 7181 (2015).
[65] S. Jaiswal, M. Ripoll, and S. Thakur, Diffusiophoretic Brownian dynamics: Characterization of hydrodynamic effects for an active chemoattractive polymer, Macromolecules **57**, 6968 (2024).
[66] N. Jain and S. Thakur, Collapse dynamics of chemically active flexible polymer, Macromolecules **55**, 2375 (2022).
[67] See Supplemental Material at http://link.aps.org/supplemental/10.1103/j1lq-6phk for further details about the simulation model, progressive deformation along the polymer contour, mean squared displacement, and supporting movies.

[68] S. Roca-Bonet and M. Ripoll, Self-phoretic Brownian dynamics simulations, Eur. Phys. J. E **45**, 25 (2022).

[69] R. K. Pathria, *Statistical Mechanics* (Elsevier, London, UK, 2016).

[70] L. Qiao and R. Kapral, Control of active polymeric filaments by chemically powered nanomotors, Phys. Rev. Appl. **18**, 024051 (2022).

[71] L. Sappl, C. N. Likos, and A. Zöttl, Polymer thermophoresis by mesoscale simulations, Macromolecules **57**, 11534 (2024).

[72] L. Sappl, C. N. Likos, and A. Zöttl, Locally tuned hydrodynamics of active polymer chains, J. Chem. Phys. **163**, 184901 (2025).

[73] L. Natali, L. Caprini, and F. Cecconi, How a local active force modifies the structural properties of polymers, Soft Matter **16**, 2594 (2020).

[74] J.-X. Li, S. Wu, L.-L. Hao, Q.-L. Lei, and Y.-Q. Ma, Nonequilibrium structural and dynamic behaviors of polar active polymer controlled by head activity, Phys. Rev. Res. **5**, 043064 (2023).

[75] S. Majumder and S. Paul, Unusual swelling and anomalous block diffusion of di- and tri-block copolymers made of active and passive monomers, J. Chem. Phys. **163**, 024907 (2025).

[76] M. Doi, S. F. Edwards, and S. F. Edwards, *The Theory of Polymer Dynamics* (Oxford University Press, Oxford, UK, 1988), Vol. 73.

[77] S. Paul, S. Majumder, and W. Janke, Activity mediated globule to coil transition of a flexible polymer in a poor solvent, Soft Matter **18**, 6392 (2022).

[78] M. Foglino, E. Locatelli, C. A. Brackley, D. Michieletto, C. N. Likos, and D. Marenduzzo, Non-equilibrium effects of molecular motors on polymers, Soft Matter **15**, 5995 (2019).

[79] S. Paul, S. Majumder, S. K. Das, and W. Janke, Effects of alignment activity on the collapse kinetics of a flexible polymer, Soft Matter **18**, 1978 (2022).

[80] A. Zöttl and H. Stark, Emergent behavior in active colloids, J. Phys.: Condens. Matter **28**, 253001 (2016).

[81] J. R. Howse, R. A. L. Jones, A. J. Ryan, T. Gough, R. Vafabakhsh, and R. Golestanian, Self-motile colloidal particles: From directed propulsion to random walk, Phys. Rev. Lett. **99**, 048102 (2007).

[82] Jülich Supercomputing Centre, JURECA: Data centric and booster modules implementing the modular supercomputing architecture at Jülich supercomputing centre, J. Large Scale Res. Facil. **7**, A182 (2021).